AIP Advances

Heat transport by phonons and the generation of heat by fast phonon processes in ferroelastic materials

X. Ding and E. K. H. Salje

Citation: AIP Advances **5**, 053604 (2015); doi: 10.1063/1.4921899
View online: http://dx.doi.org/10.1063/1.4921899
View Table of Contents: http://scitation.aip.org/content/aip/journal/adva/5/5?ver=pdfcov
Published by the AIP Publishing

Heat transport by phonons and the generation of heat by fast phonon processes in ferroelastic materials

X. Ding[1] and E. K. H. Salje[2]
[1]*State Key Laboratory for Mechanical Behavior of Materials, Xi'an Jiaotong University, Xi'an 710049, P. R. China*
[2]*Department of Earth Sciences, University of Cambridge, Cambridge, UK*

(Received 27 January 2015; accepted 18 May 2015; published online 27 May 2015)

Thermal conductivity of ferroelastic device materials can be reversibly controlled by strain. The nucleation and growth of twin boundaries reduces thermal conductivity if the heat flow is perpendicular to the twin wall. The twin walls act as phonon barriers whereby the thermal conductivity decreases linearly with the number of such phonon barriers. Ferroelastic materials also show elasto-caloric properties with a high frequency dynamics. The upper frequency limit is determined by heat generation on a time scale, which is some 5 orders of magnitude below the typical bulk phonon times. Some of these nano-structural processes are irreversible under stress release (but remain reversible under temperature cycling), in particular the annihilation of needle domains that are a key indicator for ferroelastic behaviour in multiferroic materials. [http://dx.doi.org/10.1063/1.4921899]

The quest for nanoscale phononic devices has opened a new perspective on solid state dynamics: while classic phonons are typically investigated as a bulk property, the new aspect of phononics is that they are heavily influenced by changes of nano-structures of the host lattice and are hence tunable by twinning, dislocations, and phase changes as in Mott systems.[1–5] The difference between the bulk structure and the nano-structured matrix becomes blurred when the characteristic length scale of the nanostructure is as small as a few interatomic distances, in particular in elasto-caloric materials.[6,7] Ferroelastic can act as elasto-calorics and simultaneously as tunable heat conductors. In particular martensites and ferroelastic systems with strongly first order phase transitions are potentially excellent elasto-caloric devices.[6,7] This is already demonstrated for electro-caloric materials where the effect of the elastic deformation contains a similar amount of energy as the electrically driven transition. This effect is well documented in $Pb(Sc_xTi_{1-x})O_3$ which is usually discussed as a prominent electro-caloric material but has equally strong elasto-caloric properties.[1–5]

The possibility to control phonon flow promises major technological developments in acoustics and thermal management,[8,9] equivalent to transistors that control charge flows in electronic devices. Solid-state thermal switches and diodes[9] are desirable for room-temperature cooling systems based on caloric materials,[10] as losses associated with the fluids that are currently employed to exchange heat between the working body and the heat sink or the heat load, respectively, reduce the performance of existing prototypes, and therefore cooling power.[11] Also, tunable thermal conductivity may be exploited for the design of advanced thermoelectric materials[12] that display high values of the thermoelectric figure of merit $ZT = S^2\sigma T/\kappa$ over broad temperature ranges, where S, σ, and κ are the Seebeck coefficient, electrical conductivity, and thermal conductivity of the material, respectively, and T is the absolute temperature.

In recent years, a number of strategies have been exploited to demonstrate solid-state thermal diodes at room temperature.[13–17] So far, the rectification coefficients $\kappa_{high}/\kappa_{low}$ are too small for applications. Inhomogeneously mass-loaded carbon and boron nitride nanotubes[13] display values of $\kappa_{high}/\kappa_{low} \sim 1$ (1.02 for carbon nanotubes, 1.07 for boron nitride nanotubes), whereas few-layer

graphite with asymmetric shapes display values $\kappa_{high}/\kappa_{low} < 2$ (1.28 for triangular-shaped specimens,[16] 1.6 for Y-shaped specimens[17]). Passive thermal rectification has been also demonstrated in bulk materials made of two oxides with different thermal conductivities,[14] but $\kappa_{high}/\kappa_{low} = 1.46$ as an optimum case.[15]

Li et al.[18] have argued that as the thermal conductivity is proportional to the mean free path of phonons as $\kappa = \Lambda C v/3$ (Λ is the mean free path, C is the heat capacity, v is the acoustic velocity). The mean free path is determined by two different phonon scattering events, namely (a) phonon-phonon collision and (b) interactions of phonons and twin boundaries(TBs). The effective Λ is

$$\frac{1}{\Lambda} = \frac{1}{\Lambda_{P-P}} + \frac{1}{\Lambda_{P-TB}}$$

where Λ_{P-P} and Λ_{P-TB} are the characteristic lengths of the bulk phonon-phonon scattering and the phonon-TBs scattering. The magnitude of Λ_{P-P} in ferroelastic materials can be of the order of 0.1 micrometers at low temperature,[19] which is much larger than Λ_{P-TB} here. Thus, Λ_{P-TB} can play the dominant role in determining the total mean free path Λ. For a constant Λ_{P-P}, $1/\kappa$ should be proportional to $1/\Lambda_{P-TB}$ ($1/\kappa \propto 1/\Lambda_{P-TB}$). On the other hand, here Λ_{P-TB} should be equal to the average twin boundary spacing (d), which is inversely proportional to the density of vertical twin boundaries (VTBs) $d = 1/\rho_{VTB}$. Therefore, we can finally obtain an approximate relationship of $1/\kappa$ and ρ_{VTB} as[18]

$$\frac{1}{\kappa} \propto \rho_{VTB}$$

MD simulation showed that within the strain range of 1.2–1.8% for different strain states the data fit the linear relationship between $1/\kappa$ and ρ_{VTB} very well. The key parameter is hence the domain wall density which determines the heat transport through the sample (x direction in Fig. 1(a)). Twin densities of $0.1a^{-1}$ (i.e. twin walls separated by 10 unit cells, a is the lattice unit) are plausible in view of wall separations of 15 nm (some 40 unit cells) in $SrTiO_3$ when the walls are thermally induced.[20] Cold shearing leads to higher wall densities (Fig. 1(b)) so that device applications become very likely to be located in the light blue triangle in Fig. 2. At a density of $0.1a^{-1}$ in light blue triangle, $1/\kappa = 0.015$ r.u. which is larger by a factor of 22 than the equivalent bulk value. An upper limit of the effect can be estimated when the twin density increases to $0.16a^{-1}$. The simulate contrast of the thermal conductivity reaches a factor $\kappa_{high}/\kappa_{low} = 30$ in this case. However, it should be emphasized that the thermal rectification is fixed for a given sized system. For example, $\kappa_{high}/\kappa_{low}$ is about 2.9 when the length in x axis $L_X = 160$a (see the black open symbols in Fig. 2).

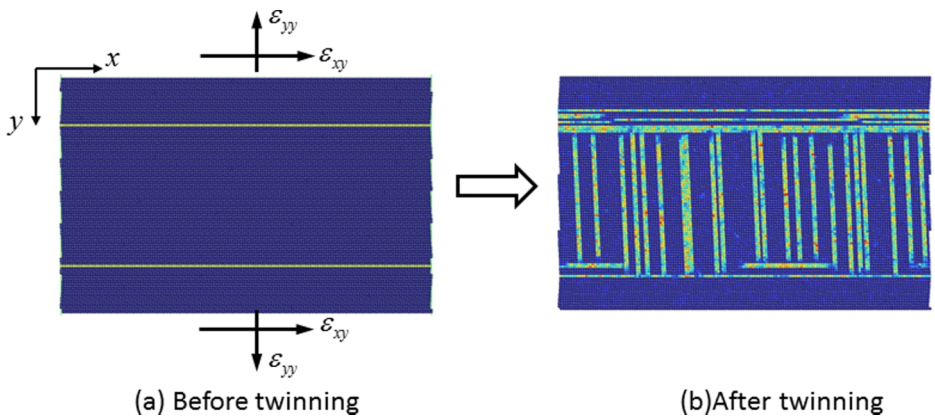

FIG. 1. A two-dimensional sandwich model with two fixed horizontal twin boundaries before twinning (a) and after twinning (b). The lattice unit is in the shape of a parallelogram with tilt angle of 4 degrees. The middle layer has an area ratio of 0.7 to the whole sample.. The deformation was performed at different strain tensor. Heat flow will be applied along x direction. Atoms are colored according to values of their centro-symmetry parameters.

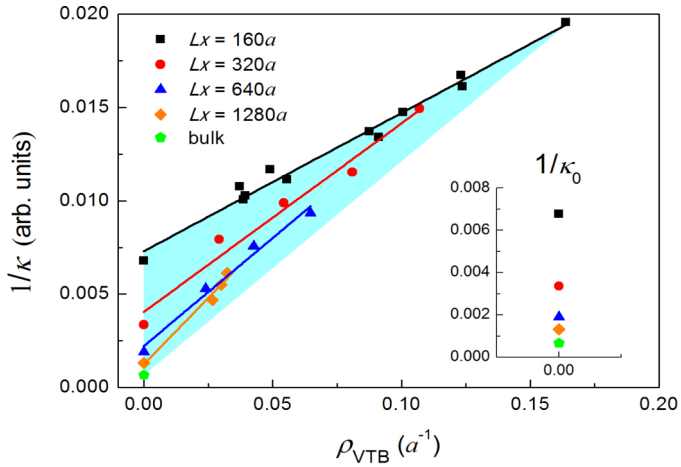

FIG. 2. The variation of thermal conductivity (κ) with twin boundary density (ρ_{VTB}) at different Lx. Reproduced with permission from Sci. Rep. **4**, 63(2014). Copyright 2014 Macmillan Publishers Limited.

Based on these results, it becomes evident that the goal of tuning thermal properties can be reached within the framework of "domain boundary engineering"[21–23] and estimate a maximum possible reduction of thermal conductivity by applied stress where the density of VTBs, which is twin boundaries that perpendicular to the heat flow (x direction in Fig. 1(a)), can be manipulated very precisely by external strain (or stress). This task becomes even easier with recently developed nanotwinned structure.[24] Since VTBs reduce thermal transport, one can hence tune thermal conductivity via the applied strain to the sample, which, in turn, can be manipulated by electric or magnetic fields in multiferroic materials.

Overall, large and reversible changes in the thermal conductivity of ferroelastic materials can be achieved by applied stress (or strain). By controlling magnitude and direction of the applied field, one manipulates the density of twin boundaries that are perpendicular to the direction of heat flow and act as phonon barriers. This strategy may be exploited for the implementation of fast controllable thermal devices, where heat-exchange surfaces can be largely increased by using multilayer geometries.

We now show that a similar approach also applies for the generation of heat and the limitation for high-frequency switching. The first issue concerns the time over which nano-scale phonons can generate heat. To visualise this point imagine a high-speed object which hits a martensitic or ferroelastic material: much of its energy is absorbed by the generation of twins and twin boundaries. Applications of this effect range from casings for mobile phones (which should not shatter when they fall on a concrete floor) to shock absorbers and bullet proof vests. Cosmic particles hitting a satellite are another scenario where nano-structural changes determine the damage which is strongly dependent on the velocity of the particles. The fundamental physics of this effect is that any mechanical impact will locally increase the density of the target or lead to microstructures such as dislocations, fission tracks, and crack propagation. Fast impact will emit shear waves through the material, which can lead to twinning. Shock induced twinning which has also been observed in sheared Cu[24–28] and Fe-Mn-Si-Al steels.[29] It is expected in most martensitic and ferroelastic materials and is at the center of this discussion.[5]

MD simulations by Zhang et al.[30] showed that the potential energy (Pe) evolves with increasing shear strain (e) for 3 different strain rates (in units of applied strain increment per phonon time) in Fig. 3(a). The microstructures at the different stages are shown in Fig. 3(b)-3(d). Similar pattern form for all strain rates with very different amplitudes: the initial state consists of 3 domains with 2 twin walls ((as shown in Fig. 1(a))). Before this sample is sheared to an upper yield point B, the potential energy Pe of the sample in all cases first increases quadratically with increasing external strain. At the upper yield point B, some kinks nucleate in the two twin walls and more complex twin pattern emerge for slow strain rates only. In this case, the stored potential energy rapidly

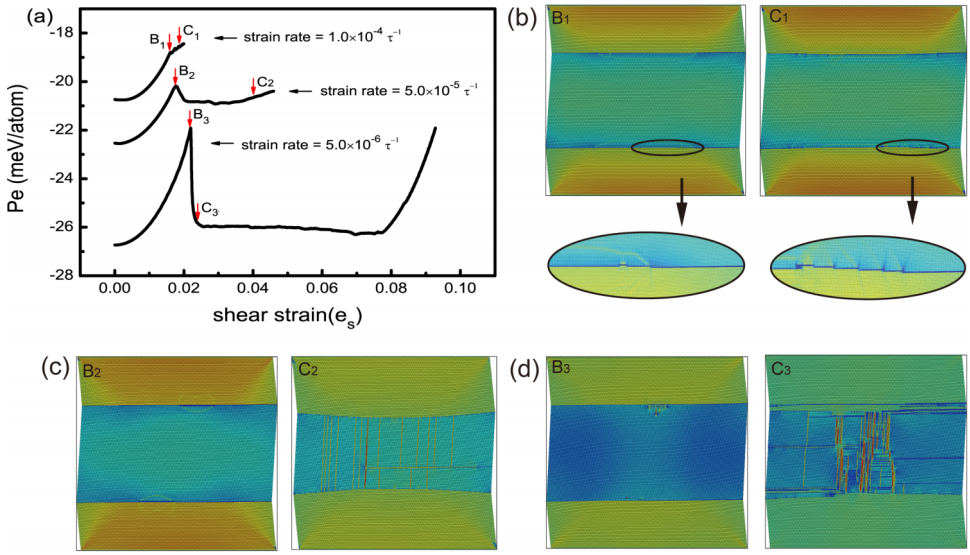

FIG. 3. (a) Evolution of the potential energy Pe with external shear strain e at three different shear strain rates (10^{-4} τ^{-1}, 5×10^{-5} τ^{-1}, 5×10^{-6} τ^{-1}). Potential energy curve of 10^{-4} τ^{-1}, 5×10^{-5} τ^{-1} is shifted upward by adding 6eV/atom and 4.2eV/atom to the original potential energy value respectively. The phonon time τ is indicated by τ to generalize the model. (b), (c), (d) are the domain structures for the yield process(B_1-C_1, B_2-C_2, B_3-C_3) at three different shear strain rates (10^{-4} τ^{-1}, 5×10^{-5} τ^{-1}, 5×10^{-6} τ^{-1}) respectively.

reduces to the lower yield point C. A complex twin pattern is formed during the microstructural transformation B_2-C_2 (or B_3-C_3). Further increase of the applied strain leads to plastic deformation and de-twinning. However, this is not the case for high strain rate, no yield behavior in the Pe versus e curve is seen (Fig. 3(a)), and only a few kink movement can be found after point B. At the highest strain , we find in all cases the onset and rapid propagation of cracks which destroy the sample.

Fig. 3 also shows that the yield behavior strongly depends on the strain rate. The energy difference between the upper and lower yield points (between points B_2-C_2 (or B_3-C_3)) is the yield energy. The yield energy is largest for low strain rates (Fig. 3(a)), with values similar to results from previous quasi- static simulations.[31–34] Increasing the strain rate decreases the yield energy from 4 meV/atom at $5\times10^{-6}\tau^{-1}$, to 0.5 meV/atom at $5\times10^{-5}\tau^{-1}$ (Fig. 3(a)), and to values smaller than 0.01 meV/atom at $10^{-4}\tau^{-1}$ (Fig. 3(a)). τ is the phonon time. The fastest strain rate in these simulations was $10^{-4}\tau^{-1}$. With a phonon time of, say, $\tau = 10^{-13}$ s, this strain rate is equivalent to $10^{9}s^{-1}$. The time to acquire a displacement of 100 nm with a typical strain of 1% and a grain size of 10 μm would then be equivalent to an impact velocity of 100 m/s. At this strain rate, the yield energy becomes zero and the impact cannot be compensated by pattern formation. The sample becomes hence inert and brittle with no damping mechanism on the time scale of the impact, besides some small kinks nucleating at the performed twin boundaries. After a small increase of strain at this rate follows nucleation and propagation of cracks. Reducing the strain rate to $5\times10^{-5}\tau^{-1}$ shows the first sign of a yield behavior where the energy reduces at the upper yield point B and a multitude of vertical twins nucleate (Fig. 3(b)). The complexity of the twin pattern does not change much with decreasing strain rate (Figs. 3(a), 3(c) and 3(d)). No shear induced twinning occurs at sufficiently high strain rates while at lower strain rates the domain pattern remains essentially invariant. For strain rates greater than $10^{-5}\tau^{-1}$, the energy absorption decreases exponentially, and the sample reacts to the impact with high inertia. Simultaneously, the impact increases the sample temperature so that the development of inertia in the pattern formation coincides with the crossover between the isothermal regime at low strain rates and an adiabatic regime at high strain rates. Samples with inertia at high strain rates (Fig. 3(a)) show cracking near the extrapolated yield point so that the sample characteristics change fundamentally from a pliable ferroelastic/martensite to a brittle ceramic. The decay in the collapse of the potential energy near the yield point is compared with the increase of phonon density and hence the temperature in the sample in Fig. 4. At high

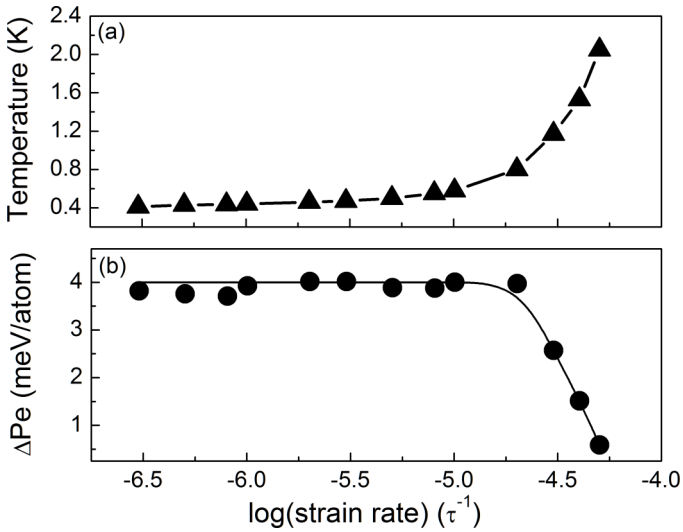

FIG. 4. The change of temperature (a) of the system and yield energy ΔPe (b) with different strain rate. ΔPe is constant at low strain rates (isothermal regime) and decays rapidly for strain rates higher than $10^{-5}\ \tau^{-1}$ (adiabatic regime). The crossover between the isothermal regime and the adiabatic regime is also observed by the heating of the sample at high strain rates.

strain rates, the sample increases its temperature by 2 K simply by an increase in phonon numbers due to impact. This transition between the isothermal and adiabatic behavior of a material plays hence an important role in the construction of elasto-caloric devices if such devices operate at high frequencies.

The second issue concerns the reversibility of nano-structural changes and their heat generation. In ferroelastic materials, the complex microstructures consist of interpenetrating twin boundaries, and it is often not possible to predict the excitation spectra of such complex patterns. Two types of observations exist for moving interfaces. When the interface relaxes under the applied strain in a continuous fashion, one observes reduced elastic moduli, elastic absorption, and changes of phase angles. Fast structural changes often correlate with the emission of mechanical spike related to strain release, such as pinning and unpinning of interfaces, the formation of cracks, etc. These effects are collectively known as "jerks" and have been investigated for almost 100 years in magnets as Barkhausen jumps or avalanches.[31,32,35–38] Their origin stems from the complexity of the domain patterns and the randomness of defects distributions. Only in simple patterns are elastic responses related to the dynamical behavior of individual twin boundaries[38–41] and will only in cases of extremely strong pinning mirror the intrinsic elastic moduli of the matrix or the composite of a matrix with finely dispersed interfaces.[42–45] Fast events related to the movement of domain boundaries are often superposed by slow events at larger forces, such as grain boundary sliding motions.[46]

MD simulations[47] identified a typical example when needle domains retract beyond a critical distance. This movement becomes irreversible when the needle becomes shorter than a well-determined length. Shorter needles shrink critically until they vanish (Fig. 5). The dissipated energy of the needle is absorbed by phonons and leads to a heating of the sample. To observe the temperature changes, we disconnect the heat bath of the MD simulation from the sample and observe which geometric change of the microstructure leads to changes of the sample temperature. In Figure 6 three typical scenarios are shown. We find no temperature change besides the statistical thermal fluctuations when the microstructure does not change (because the driving amplitudes are too low or the frequency is too high). This case is indicated as "purely elastic" in the figure. When the needle is driven strongly and retracts into the upper twin wall, i.e., when the twin wall is topologically destroyed, we find a heat jump, which represents the release of the pinning and self-energy of the needle domain. This event would macroscopically be a large "jerk" as analyzed in Salje et al.[31] In the intermediate case, the needle can progress and retract reversibly where each small depinning

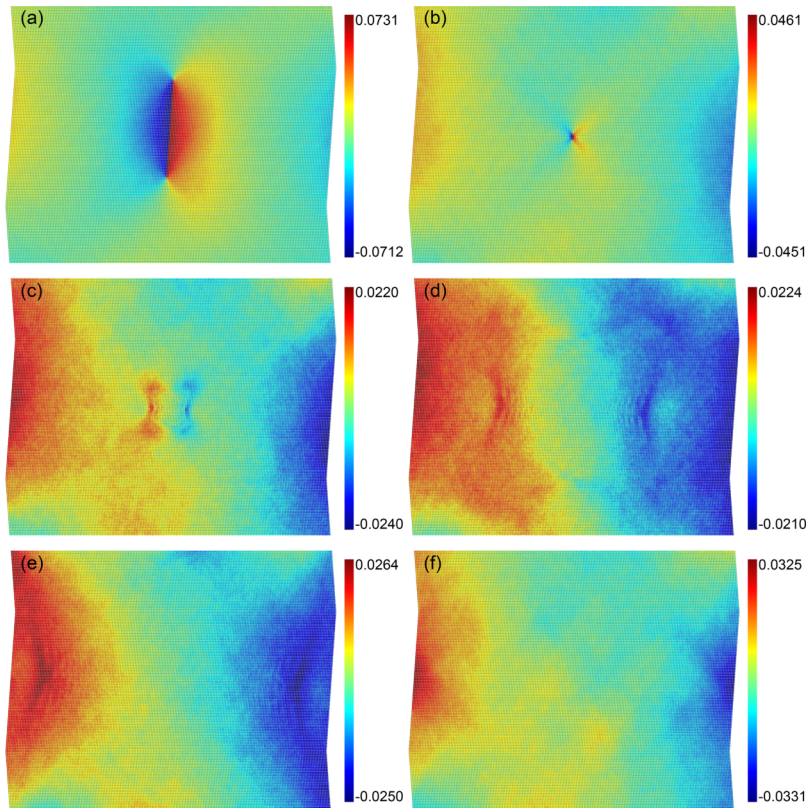

FIG. 5. Snapshots of the irreversible retraction of a needle domain under external strain and the subsequent propagation of phonons. (a) The needle first detaches at the twin boundaries. (b) The total length of the needle then reduces very quickly and disappears. In c-e, the strain energy, which was absorbed by the needle is now released into the lattice and leads to changes of the atomic displacements, which propagate as phonon excitations. Ultimately, in panel f, the sample will relax to the initial configuration but without the needle domain.

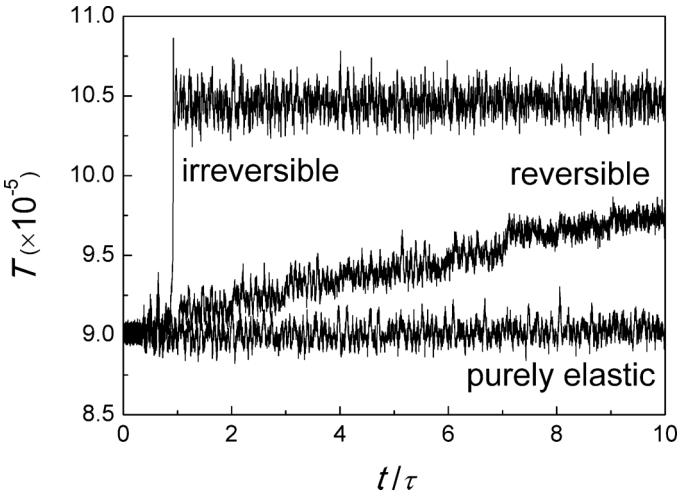

FIG. 6. Sample heating by moving needles domains (temperature T in MD units, t is time, and τ is phonon time). During the irreversible disappearance of the needle a large temperature jump is seen, which corresponds to a jerk in the energy content of the sample. In purely elastic movements, very little heat is transferred and an almost continuous heating of the sample stems from oscillating needles (in reversible movements). Reproduced with permission from American Mineralogist **98**, 1449 (2013). Copyright 2013 the Mineralogical Society of America.

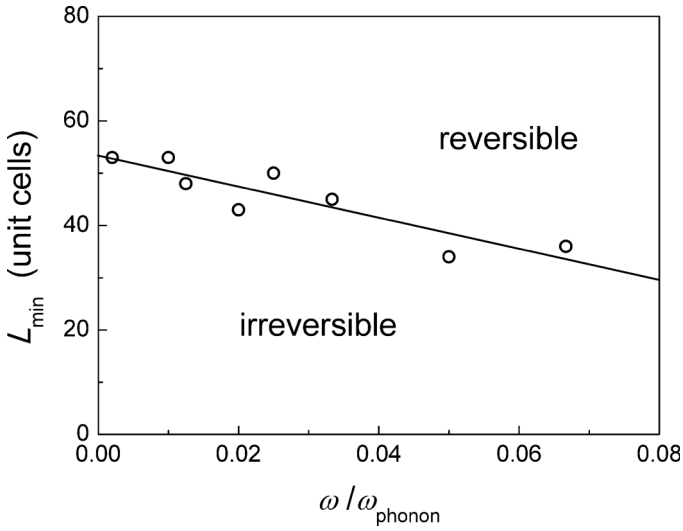

FIG. 7. Phase boundary between the reversible and irreversible phase shown as function of frequency ω (ω_{phonon} is the frequency of phonon) and the minimum needle length beyond which the needle domain will destruct. The total distance between the anchoring twin walls is 100 lattice lengths, the typical critical needle length is 50 lattice lengths or half the distance between the twin walls. Reproduced with permission from American Mineralogist **98**, 1449 (2013). Copyright 2013 the Mineralogical Society of America.

process leads to a heat release followed by a short plateau in which only thermal fluctuations occur. The repeated retraction and progression of the needle will then heat the sample in an almost continuous fashion. Macroscopically, this case corresponds to friction heating by needle oscillations.

This effect defines two scenarios, namely one for the reversible needle retraction and one for the irreversible retraction. The critical needle length defines the irreversibility line as function of the frequency of the applied oscillatory strain. The frequency dependence stems from the fact that the needle can follow the strain only at low frequencies while at high frequencies the needle movement is retarded and cannot follow the external oscillation. If we now consider the needle length itself, we can construct a phase diagram (Fig. 7) as a function of the needle length vs. frequency. The characteristic critical needle length is 50 lattice units, which is half the distance between the bordering twin walls. As shown in Fig. 7 the critical length for the transition to the irreversible regime decays slightly with increasing frequency. The movement becomes irreversible when the needle retracts by half its original length, namely the distance between the bordering twin walls. Similar effects were also shown for kink movements.[34] When a needle is shifted by 50 lattice units, the needle continues to shrink and disappear. These irreversible movement also means that heat is transferred to the system as a heat spike. The heat spike has been found in Ref. 30 and the results are presented there and shown directly in Fig. 4.

In summary, ferroelastic materials and most multiferroics, which are mostly strongly ferroelastic, give rise to the generation and annihilation of heat via the elasto-caloric effect. The efficiency of the materials is limited to moderately high frequencies. If the frequencies are too high we predict a crossover between isothermal and adiabatic regimes and the crossing of the irreversibility line for several nano-structures. The same materials can also be used as tunable heat conductors where the theromal conductivity depends on the density of twin boundaries perpendicular to the the heat flow.

ACKNOWLEDGEMENT

XD appreciate the support of NSFC (51171140, 51320105014, 51321003).EKHS is grateful to EPSRC (EP/K009702/1) and the Leverhulme Trust (RPG-2012-564).

[1] O. Aktas, S. Crossley, M. A. Carpenter, and E. K. H. Salje, Phys. Rev. B **90**, 16 (2014).
[2] E. Dul'kin, E. K. H. Salje, O. Aktas, R. W. Whatmore, and M. Roth, Appl. Phys. Lett. **105**, 21 (2014).
[3] J. C. Lashley, K. Gofryk, B. Mihaila, J. L. Smith, and E. K. H. Salje, J. Phys.:Condens. Matter **26**, 3 (2014).

[4] E. K. H. Salje, X. Ding, and Z. Zhao, Appl. Phys. Lett. **102**, 15 (2013).
[5] E. K. H. Salje, Annu. Rev. Mater. Res. **42**, 265 (2012).
[6] S. Fahler, U. K. Rossler, O. Kastner, J. Eckert, G. Eggeler, H. Emmerich, P. Entel, S. Muller, E. Quandt, and K. Albe, Adv. Eng. Mater. **14**, 10 (2012).
[7] M. Valant, Prog. Mater. Sci. **57**, 980 (2012).
[8] M. Maldovan, Nature **503**, 209 (2013).
[9] N. Li, J. Ren, L. Wang, G. Zhang, P. Haenggi, and B. Li, Rev. Mod. Phys. **84**, 1045 (2012).
[10] X. Moya, S. Kar-Narayan, and N. D. Mathur, Nat. Mater. **13**, 439 (2014).
[11] B. Yu, M. Liu, P. W. Egolf, and A. Kitanovski, Int. J. Refrig. **33**, 1029 (2010).
[12] H. C. Chang, C. H. Chen, and Y. K. Kuo, Nanoscale **5**, 7017 (2013).
[13] C. W. Chang, D. Okawa, A. Majumdar, and A. Zettl, Science **314**, 1121 (2006).
[14] W. Kobayashi, Y. Teraoka, and I. Terasaki, Appl. Phys. Lett. **95**, 17 (2009).
[15] D. Sawaki, W. Kobayashi, Y. Moritomo, and I. Terasaki, Appl. Phys. Lett. **98**, 8 (2011).
[16] H. Tian, D. Xie, Y. Yang, T. L. Ren, G. Zhang, Y. F. Wang, C. J. Zhou, P. G. Peng, L. G. Wang, and L. T. Liu, Sci. Rep. **2**, 523 (2012).
[17] G. Zhang and H. Zhang, Nanoscale **3**, 4604 (2011).
[18] S. Li, X. Ding, J. Ren, J. Sun, and E. K. H. Salje, Sci. Rep. **4**, 63 (2014).
[19] S. Mielcarek, B. Mroz, Z. Tylczynski, P. Piskunowicz, Z. Trybula, and M. Bromberek, Physica B **299**, 83 (2001).
[20] J. Chrosch and E. K. H. Salje, J. Phys.:Condens. Matter **10**, 2817 (1998).
[21] E. K. H. Salje and H. L. Zhang, Phase Transit. **82**, 452 (2009).
[22] E. K. H. Salje, Chem. Phys. Chem. **11**, 940 (2010).
[23] S. Van Aert, S. Turner, R. Delville, D. Schryvers, G. Van Tendeloo, and E. K. H. Salje, Adv. Mater. **24**, 523 (2012).
[24] L. Lu, X. Chen, X. Huang, and K. Lu, Science **323**, 607 (2009).
[25] F. Cao, I. J. Beyerlein, F. L. Addessio, B. H. Sencer, C. P. Trujillo, E. K. Cerreta, and G. T. Gray III, Acta Mater. **58**, 549 (2010).
[26] N. K. Bourne, J. C. F. Millett, and G. T. Gray III, J. Mater. Sci. **44**, 3319 (2009).
[27] J. Yang, J. I. Goldstein, E. R. D. Scott, J. R. Michael, P. G. Kotula, T. Pham, and T. J. McCoy, Meteorit. Planet. Sci. **46**, 1227 (2011).
[28] A. E. Rubin, Meteorit. Planet. Sci. **32**, 231 (1997).
[29] O. Grassel and G. Frommeyer, Mater. Sci. Technol. **14**, 1213 (1998).
[30] L. Zhang, E. K. H. Salje, X. Ding, and J. Sun, Appl. Phys. Lett. **104**, 162906 (2014).
[31] E. K. H. Salje, X. Ding, Z. Zhao, T. Lookman, and A. Saxena, Phys. Rev. B **83**, 10 (2011).
[32] X. Ding, Z. Zhao, T. Lookman, A. Saxena, and E. K. H. Salje, Adv. Mater. **24**, 5385 (2012).
[33] X. Ding, T. Lookman, Z. Zhao, A. Saxena, J. Sun, and E. K. H. Salje, Phys.Rev. B **87**, 9 (2013).
[34] Z. Zhao, X. Ding, T. Lookman, J. Sun, and E. K. H. Salje, Adv. Mater. **25**, 3244 (2013).
[35] D. Spasojevic, S. Bukvic, S. Milosevic, and H. E. Stanley, Phys. Rev. E **54**, 2531 (1996).
[36] A. P. Mehta, A. C. Mills, K. A. Dahmen, and J. P. Sethna, Phys. Rev. E **65**, 4 (2002).
[37] J. P. Sethna, K. A. Dahmen, and C. R. Myers, Nature **410**, 242 (2001).
[38] E. K. H. Salje, X. Ding, Z. Zhao, and T. Lookman, Appl. Phys. Lett. **100**, 22 (2012).
[39] E. K. H. Salje, Phys. Chem. Miner. **35**, 321 (2008).
[40] E. K. H. Salje and H. L. Zhang, Phase Transit. **82**, 452 (2009).
[41] E. K. H. Salje and H. L. Zhang, J. Phys.:Condens. Matter **21**, 3 (2009).
[42] W. T. Lee, E. K. H. Salje, L. Goncalves-Ferreira, M. Daraktchiev, and U. Bismayer, Physi. Rev. B **73**, 21 (2006).
[43] L. Goncalves-Ferreira, S. A. T. Redfern, E. Atacho, and E. K. H. Salje, Appl. Phys. Lett. **94**, 8 (2009).
[44] E. K. H. Salje, J. Koppensteiner, M. Reinecker, W. Schranz, and A. Planes, Appl. Phys. Lett. **95**, 23 (2009).
[45] M. Calleja, M. T. Dove, and E. K. H. Salje, J. Phys.:Condens. Matter **15**, 2301 (2003).
[46] S. J. S. Morris and I. Jackson, J. Mech. Phys. Solids **57**, 744 (2009).
[47] E. K. H. Salje, Z. Zhao, X. Ding, and J. Sun, American Mineralogist **98**, 1449 (2013).